UNDRAINED SHEAR STRENGTH OF PLASTIC SILT SUBJECT TO BLAST-INDUCED EXCESS PORE PRESSURES

Bridge Section

PROJECT WO#18-11

Oregon Department of Transportation

UNDRAINED SHEAR STRENGTH OF PLASTIC SILT SUBJECT TO BLAST-INDUCED EXCESS PORE PRESSURES

Bridge Section

PROJECT WO#18-11

by
Armin W. Stuedlein, Ph.D., P.E. (WA)
Professor, Geotechnical Engineering

Amalesh Jana
Graduate Research Assistant

Aleyna Donaldson
Graduate Research Student

for

Oregon Department of Transportation
Research Section
555 13th Street NE, Suite 1
Salem OR 97301

December 2021

Technical Report Documentation Page

1. Report No. OR-RD-22-09	2. Government Accession No.	3. Recipient's Catalog No.
4. Title and Subtitle Undrained Shear Strength of Plastic Silt Subject to Blast-induced Excess Pore Pressures		5. Report Date December 2021 6. Performing Organization Code
7. Author(s) Armin W. Stuedlein, Ph.D., P.E. (WA), 0000-0002-6265-9906 Amalesh Jana, 0000-0003-1130-4037 Aleyna Donaldson		8. Performing Organization Report No.
9. Performing Organization Name and Address Oregon Department of Transportation Research Section 555 13th Street NE, Suite 1 Salem, OR 97301		10. Work Unit No. (TRAIS) 11. Contract or Grant No.
12. Sponsoring Agency Name and Address Oregon Dept. of Transportation Research Section 555 13th Street NE, Suite 1 Salem, OR 97301		13. Type of Report and Period Covered Final Report 14. Sponsoring Agency Code
15. Supplementary Notes		

16. Abstract:

This research report evaluates the undrained shear strength of plastic silts soils subject to raised excess pore pressures such as those resulting from strong ground motion. The knowledge of the possible reduction in undrained shear strength of soils is useful for planning and executing construction of transportation infrastructure subject to earthquake shaking. The results of this study showed that for excess pore pressures equal to 12.6 to 17.5% of the in situ vertical effective overburden stress, the plastic silt deposit forming the subject of this investigation resulted in a loss of undrained shear strength ranging from 44 to 50%. The post-blasting undrained shear strength associated with the raised excess pore pressure field was determined equal to the initial, residual undrained shear strength as observed using the vane shear test.

17. Key Words	18. Distribution Statement Copies available from NTIS, and online at www.oregon.gov/ODOT/TD/TP_RES/		
19. Security Classification (of this report) Unclassified	20. Security Classification (of this page) Unclassified	21. No. of Pages 54	22. Price

SI* (MODERN METRIC) CONVERSION FACTORS

APPROXIMATE CONVERSIONS TO SI UNITS

Symbol	When You Know	Multiply By	To Find	Symbol
		LENGTH		
in	inches	25.4	millimeters	mm
ft	feet	0.305	meters	m
yd	yards	0.914	meters	m
mi	miles	1.61	kilometers	km
		AREA		
in^2	square inches	645.2	millimeters squared	mm^2
ft^2	square feet	0.093	meters squared	m^2
yd^2	square yards	0.836	meters squared	m^2
ac	acres	0.405	hectares	ha
mi^2	square miles	2.59	kilometers squared	km^2
		VOLUME		
fl oz	fluid ounces	29.57	milliliters	ml
gal	gallons	3.785	liters	L
ft^3	cubic feet	0.028	meters cubed	m^3
yd^3	cubic yards	0.765	meters cubed	m^3
~NOTE: Volumes greater than 1000 L shall be shown in m^3.				
		MASS		
oz	ounces	28.35	grams	g
lb	pounds	0.454	kilograms	kg
T	short tons (2000 lb)	0.907	megagrams	Mg
		TEMPERATURE (exact)		
°F	Fahrenheit	(F-32)/1.8	Celsius	°C

APPROXIMATE CONVERSIONS FROM SI UNITS

Symbol	When You Know	Multiply By	To Find	Symbol
		LENGTH		
mm	millimeters	0.039	inches	in
m	meters	3.28	feet	ft
m	meters	1.09	yards	yd
km	kilometers	0.621	miles	mi
		AREA		
mm^2	millimeters squared	0.0016	square inches	in^2
m^2	meters squared	10.764	square feet	ft^2
m^2	meters squared	1.196	square yards	yd^2
ha	hectares	2.47	acres	ac
km^2	kilometers squared	0.386	square miles	mi^2
		VOLUME		
ml	milliliters	0.034	fluid ounces	fl oz
L	liters	0.264	gallons	gal
m^3	meters cubed	35.315	cubic feet	ft^3
m^3	meters cubed	1.308	cubic yards	yd^3
		MASS		
g	grams	0.035	ounces	oz
kg	kilograms	2.205	pounds	lb
Mg	megagrams	1.102	short tons (2000 lb)	T
		TEMPERATURE (exact)		
°C	Celsius	1.8C+32	Fahrenheit	°F

*SI is the symbol for the International System of Measurement

ACKNOWLEDGEMENTS

The authors gratefully acknowledge the Cascadia Lifelines Program (CLiP) and its members, with special thanks to member agency Port of Portland and Oregon Department of Transportation. The research presented within this work was made possible by the vision and leadership of Tom Wharton, P.E. (OR) of the Port of Portland, and Susan Ortiz, P.E.(OR) and Kira Glover-Cutter, Ph.D., of the Oregon Department of Transportation. Thanks are due to the following Oregon State University professional faculty, staff, and students who engaged in discussions and/or assisted with various portions of the work: T. Matthew Evans, James Batti, Jeff Gent, Erick Moreno-Rangel, and Ali Dadashi.

DISCLAIMER

TABLE OF CONTENTS

LIST OF TABLES

LIST OF FIGURES

1.0 INTRODUCTION

Recent subduction zone earthquakes, including the 2010 Maule, Chile and 2011 Tohoku, Japan earthquakes, have gained significant attention due to their strong intensity of shaking and long duration. The Cascadia Subduction Zone, running 1,000 km from Northern California in the south to British Columbia in the north, last ruptured on 26 January 1700 with an estimated moment magnitude of ~9.0, and produced a tsunami that resulted in thousands of deaths and casualties as far away as Japan (Atwater et al. 2004). On the basis of turbidite deposits off the Pacific Northwest coastline, Goldfinger et al. (2012) estimated that the likelihood of the next Cascadia earthquake ranges from 7 to 12% and 37 to 42% in 50 years for the northern and southern margins of the subduction zone, respectively. Accordingly, significant interest in improving seismic resiliency has increased by the owners of civil infrastructure, including departments of transportation and ports.

As part of its long-term resilience goals, the Port of Portland, located in Portland, Oregon, has determined that one of its two runways must be hardened against the vertical and lateral deformations anticipated following rupture of the Cascadia Subduction Zone and the nearby, though smaller, Port Hills fault. A portion or all of both runways lie in close proximity to the Columbia River, which has been dredged to maintain shipping freighters to depths as great as 20 m. Lateral spreading has been determined to pose a significant risk to the runways, given that the subsurface consists of dredge sand fill, medium stiff silt, and a deep deposit of medium dense sand. Prior to selecting and executing a costly ground improvement program, the Port has determined that an improved understanding of the cyclic resistance of the silt and sand deposits is warranted. Deep, in-situ blast liquefaction experiments conducted by Oregon State University served to provide a means to understand the seismic performance of these soils without the possible effects of sample disturbance, small sample-size effects, artificial drainage conditions, and under existing mechanical, hydrogeological, and thermal conditions.

Of particular importance for the evaluation of global stability of structures founded within or above plastic soils is the need to understand the possible magnitude of cyclic softening of plastic soils under earthquake loading. Cyclic softening is associated with the development of excess pore pressures under vertically-propagating horizontal shear waves derived from the rupture of faults. The deep, in-situ blasting program included the evaluation of a thick deposit of plastic silt, and presented the opportunity to measure the undrained shear strength associated with a raised excess pore pressure field. This report presents the test site and subsurface conditions, the experimental protocols necessary to conduct *in situ* measurements of undrained shear strength, and the results of the pre- and post-blast undrained shear strength of plastic silt to evaluate the magnitude of reduction in undrained shear strength.

2.0 SITE AND SUBSURFACE DESCRIPTION

2.1 OVERVIEW OF TEST SITE AND SUBSURFACE CONDITIONS

The blast-liquefaction test site is located on the grounds of Portland International Airport, owned and operated by the Port of Portland, and situated approximately 1.2 km southeast of, and aligned with, the South Runway. Initial cone penetration tests (CPTs) and borings indicated the suitability of this site for the purposes of conducting a controlled blasting experiment, as well as its sufficient distance from nearby structures. Figures 2.1 presents an aerial photograph indicating the situation of the test site and 150' long blast array, whereas Figure 2.2 presents the site and exploration plan, as well as relevant components of the experiments, including blast casings, pore pressure transducers (PPTs), and velocity transducers. The first ten blast casings (starting from the west) extended to approximately 27 m depth and were used to excite the deep instrumentation array (Figure 2.3), whereas the five blast casings located along the eastern end of the site extended to a depth of approximately 12 m and were used, along with the five middle casings, to excite the shallow instrumentation array.

CPTs conducted along the array alignment, as well as mud-rotary borings performed for split-spoon sampling and penetration testing, were used to construct the subsurface model of the test site presented in Figure 2.3 (see Appendix A for the corresponding logs). Dredge sand and silty sand fill comprises the upper 5 to 6 m of the subsurface, and is underlain by a +/- 2 m thick layer of native, alluvial, loose, clean SAND. Below the native sand deposit lies a 5 to 6 m thick alluvial, medium stiff, clayey SILT deposit with traces of sand and thin stringers of sandy SILT. Extending below the silt layer and to the depth of the explorations lies a deep deposit of alluvial, medium dense, clean SAND. As indicated in Figure 2.3, the deep and shallow arrays were installed at depths where the CPTs indicated the most uniform conditions exist, though variations in relative density (deep array) and consistency (shallow array) were noted during sampling at the instrument locations.

Figure 2.1. Aerial photograph indicating location of the 150' long blast array aligned along due East and West.

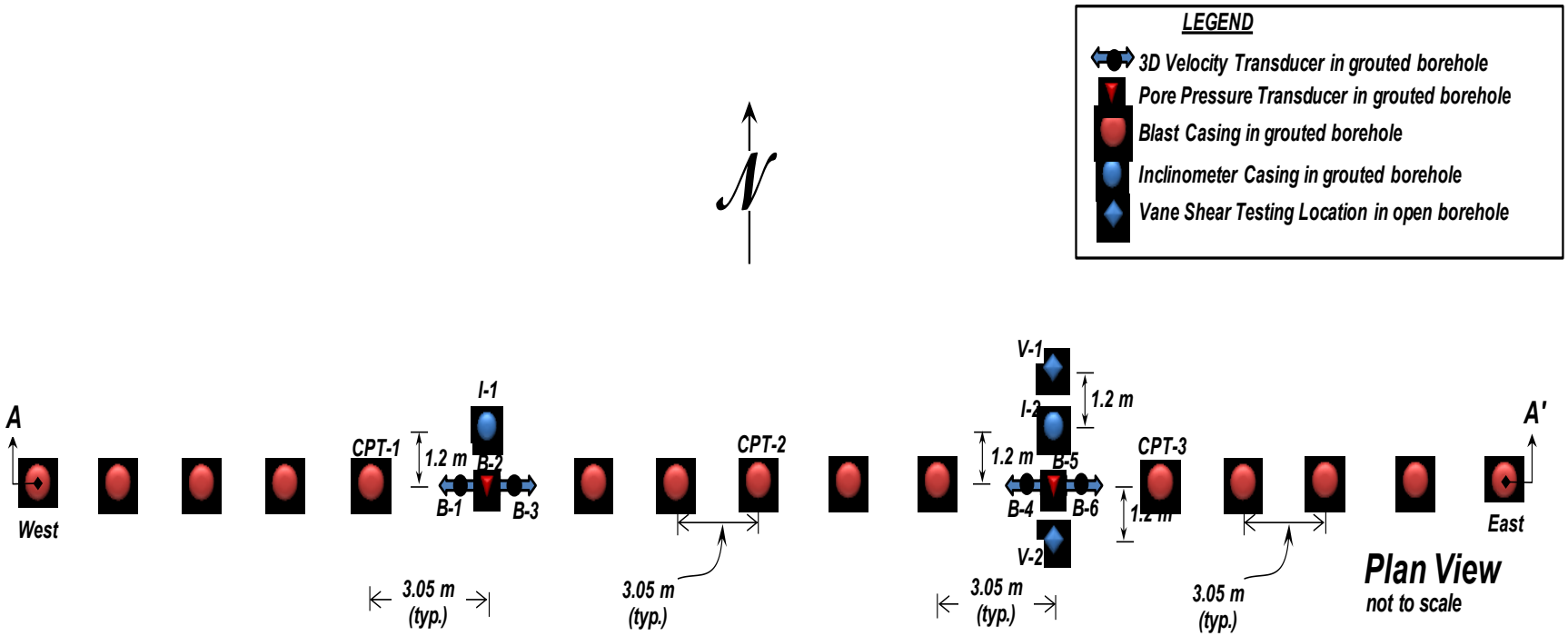

Figure 2.2. Site and exploration plan showing explorations and instrumentation arrays aligned along due East and West.

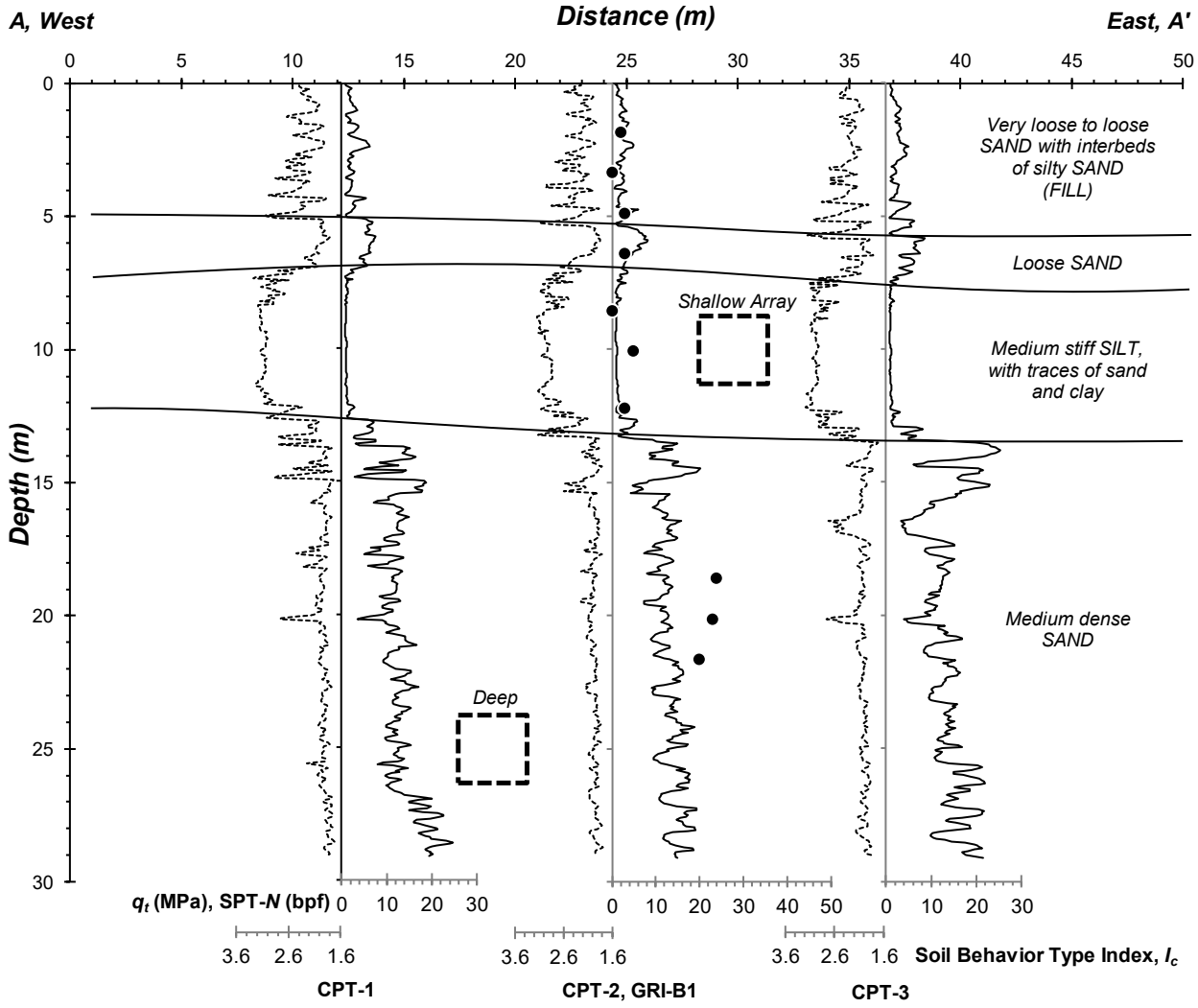

Figure 2.3. Subsurface cross-section A-A' showing a portion of the explorations, and depth and extent of the deep and shallow arrays used to observe the response to controlled blasting

2.2 PRELIMINARY GEOTECHNCIAL CHARACTERIZATION OF THE SILT LAYER

The Port of Portland engaged the services of Geotechnical Resources, Inc. (GRI) to evaluate several potential test sites for the blast liquefaction experiments. Several borings and one CPT performed at the test site selected had indicated that site exhibited similar characteristics to the general stratigraphy underlying the Port property and was deemed suitably representative. Laboratory index test data provided by GRI indicated that the silt layer exhibited significant variability, but generally demonstrated that the silt was of low plasticity and thus potentially susceptible to liquefaction under the "sand-like" paradigm (e.g., Boulanger and Idriss 2006). The plastic index, *PI*, defined as the range of water content over which sand exhibits plastic behavior, generally ranged from 4 to 14, with corresponding USCS classification of ML, with one sample exhibiting an PI equal to 70 (corresponding to USCS classification CH or fat clay), as shown in

Figures 2.4 and 2.5. The laboratory tests also indicated that the water content was similar or equal to the liquid limit, *LL*, indicating that the soil was lightly overconsolidated to normally-consolidated. These laboratory results suggested that the potential for large shear strain under cyclic loading was large and that significant pore pressure generation could be expected under the Cascadia Subduction Zone or Port Hills Fault rupture scenarios.

During the installation of instruments necessary to conduct the blast liquefaction, intact Shelby tube samples were retrieved from the middle of the silt layer and transported to Oregon State University for laboratory testing. The results of index testing indicated that at the location of the instrumented array (approximately 30 m or 100 ft south of the GRI explorations), the plasticity of the silt was significantly higher. Figures 2.4 and 2.5 show that the *PI* determined using ASTM standards and alternative fall cone tests typically ranged from 17 to 31 and 21 to 34, respectively. Similar to GRI, the water content was similar to or equal to the *LL*, however the liquid limit was significantly higher at the array location and depth. Using typical liquefaction screening criteria, the silt soil was deemed insusceptible to liquefaction under the "sand-like" paradigm and may rather be susceptible to cyclic softening, as described in Section 4.2. It is noted that silts with the plasticity observed in OSUs borings have been encountered by ODOT in the general area of the test site location, but are significantly less common than the silts with plasticity reported by GRI, Inc. for their boring location. Figure 2.6 presents the results of hydrometer tests, providing particle size distributions for samples retrieved from the silt layer within the instrumented depths. The samples tested indicate zero sand content (threshold particle size of 0.074 mm) and 10 to 17% clay content (with threshold particle size of 0.001 mm). The CPT data presented in Figure 2.3 and index test data presented in Figures 2.4 through 2.5 should be compared to other silt soils of concern to ODOT when considering the results of the vane shear tests described in Section 4.

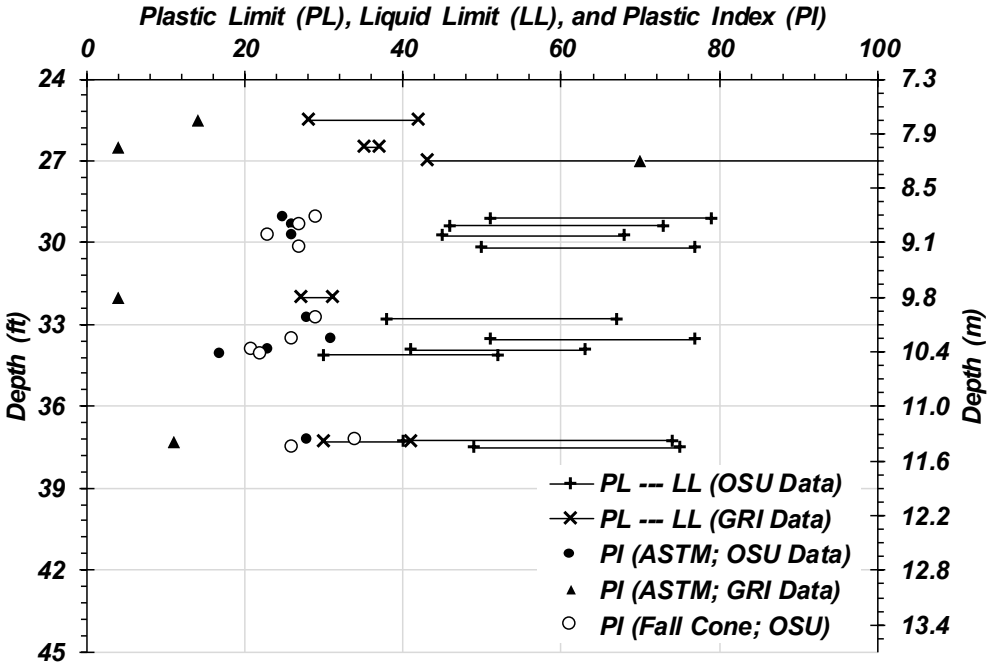

Figure 2.4. Depth variation of Atterberg Limits (PL, LL), and plastic index (PI) from samples tested to date by OSU and GRI, Inc

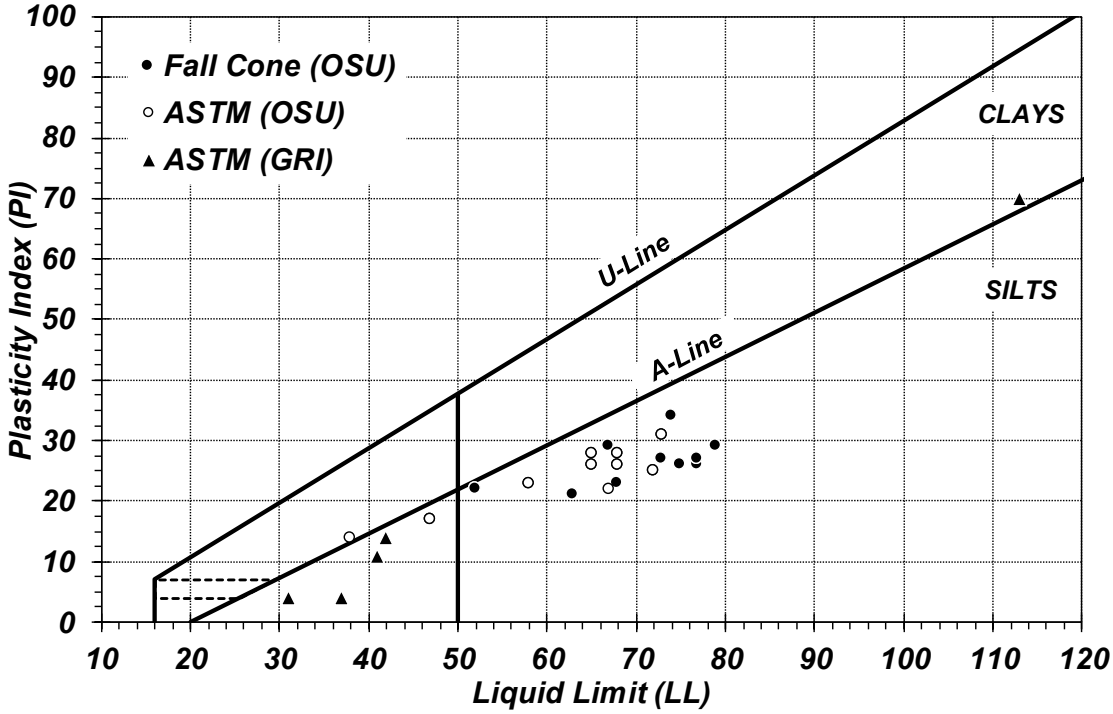

Figure 2.5. Plasticity chart with data from Figure 2.4

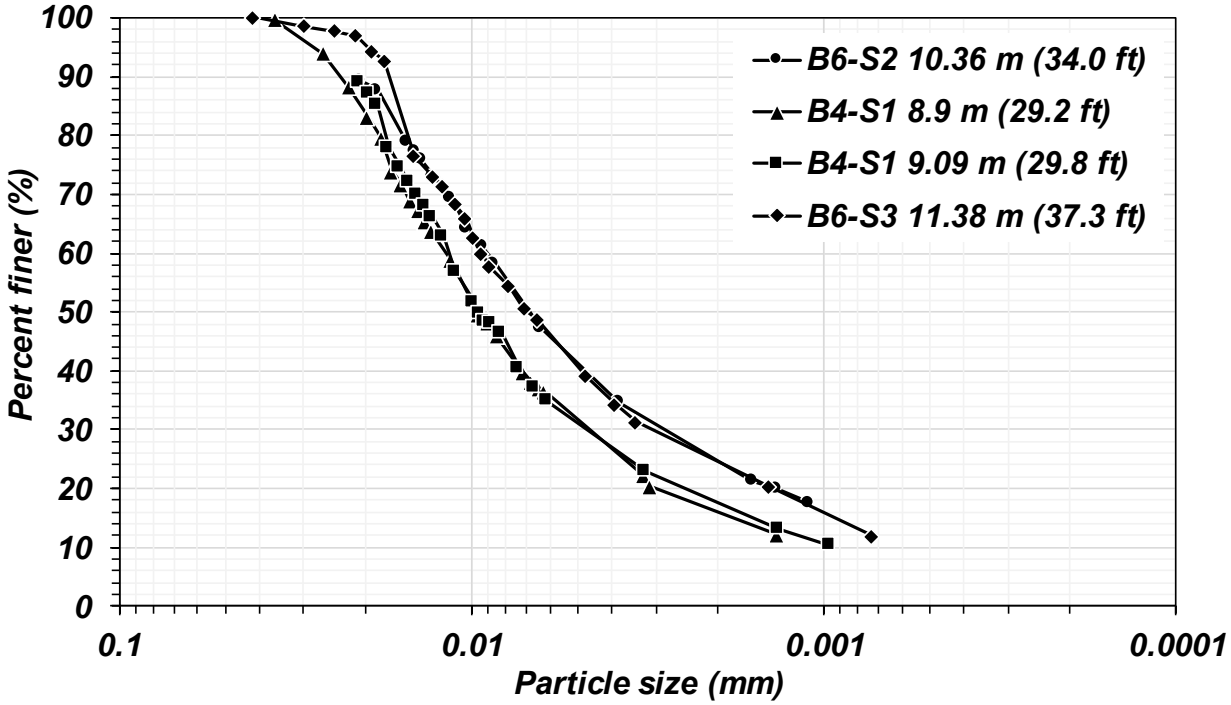

Figure 2.6. Particle size distribution of samples retrieved from the instrumented depths

3.0 EXPERIMENTAL PROTOCOLS

3.1 OVERVIEW OF INSTRUMENTATION USED

Instruments necessary to capture the in-situ response to controlled blasting were installed within 8" mud-rotary boreholes to form the deep and shallow array (Figure 3.1) and were accompanied by ground surface monitoring monuments (not discussed herein). Each array consisted of a minimum of four boreholes: (1) one to house full-depth inclinometer casing fitted with sondex settlement rings to capture post-liquefaction volumetric strain, (2) one to house the pore pressure transducer (PPT) string, and (3) two boreholes to place the triaxial geophone packages (TGPs), each of which consist of triaxial velocity transducers and a six-axis accelerometer gyroscope to capture static tilt. Figure 5 presents the intended array geometry, designed to allow deduction of the change in shear modulus and excess pore pressure with imposed shear strain following the approach implemented by Suits et al. (2009) and van Ballegooy et al. (2015). Note that instruments were placed with minor deviations from that intended. Due to the pre-installation uncertainty of borehole deviation, sensor packages were suspended from inclinometer casings to assist in determining the post installation locations, the determination of which was guided by the adjacent full-depth inclinometer casing that accompanied each array. The TGPs and PPTs were installed with the aid of weights to allow placement through the heavy drilling fluid specified and to plumb the sensors under gravity. Each type of instrumentation, and the installation thereof, required careful calibration in order to ensure that accurate voltage-to-amplitude conversions could be obtained and that the location and orientation of each instrument could be accurately ascertained. The remainder of this report focuses on the procedures used to observe the pore pressures associated with controlled blasting to provide a basis for interpretation of the VST data.

3.2 PORE PRESSURE TRANSUCERS (PPTS) USED TO MONITOR BLAST-INDUCED EXCESS PORE PRESSURES

3.2.1 General Characteristics of PPTs

Pore pressure transducers (PPTs) measure hydrostatic and hydrodynamic water pressure, u. These pressure transducers can indicate where the ground water table is located or piezometric levels in unconfined and confined aquifers, respectively, and measure the hydrodynamic and residual excess pore pressures induced by blasting. In order to measure excess pore pressures induced by blasting, the PPT should withstand a blast pressure of up to 41 MPa (for the experiments considered in the study) and be able to measure pressure changes as small as 690 Pa (Rollins et al. 2005, Rollins and Anderson 2008). The Druck Unik 5000 PMP5034-TA-A3-CA-HO-PF was selected to meet these requirements. Each amplified pressure transducer consists of a stainless steel body and a small diaphragm chamber placed at its bottom (Figure 3.2). The PPTs are capable of measuring pressure ranges of 0 to 5.2 MPa, and withstanding blast pressures up to 20.7 MPa (General Electric Oil & Gas, 2009), which was considered sufficient for the experimental design used in this study (verified following the experiments). The PPT body

measures 83 mm in length and 25 mm in diameter. While each PPT was designed to withstand large pressures, the sensitivity of each PPT's internal sensor required that each PPT be placed into a custom made housing to prevent the PPT from being damaged by blasting pressures and prevent soil and grout from entering the diaphragm chamber of the PPT. The housings used at the test site were the same as those described by Gianella (2015) and Gianella and Stuedlein (2017). Figure 3.2 presents the acrylic housing, which was 20.3 cm long and has an outside diameter of 5.1 cm, and a wall thickness or 0.63 cm. Porous bronze filters secured into the side of the housing to prevent soil and grout from entering the housing, and to allow communication of pressures between the outside and inside of the housing. To improve accuracy of the pore pressure measurements, the PPT diaphragm is placed three-fourths of the way into the housing so that the diaphragm chamber was level with the bronze filters.

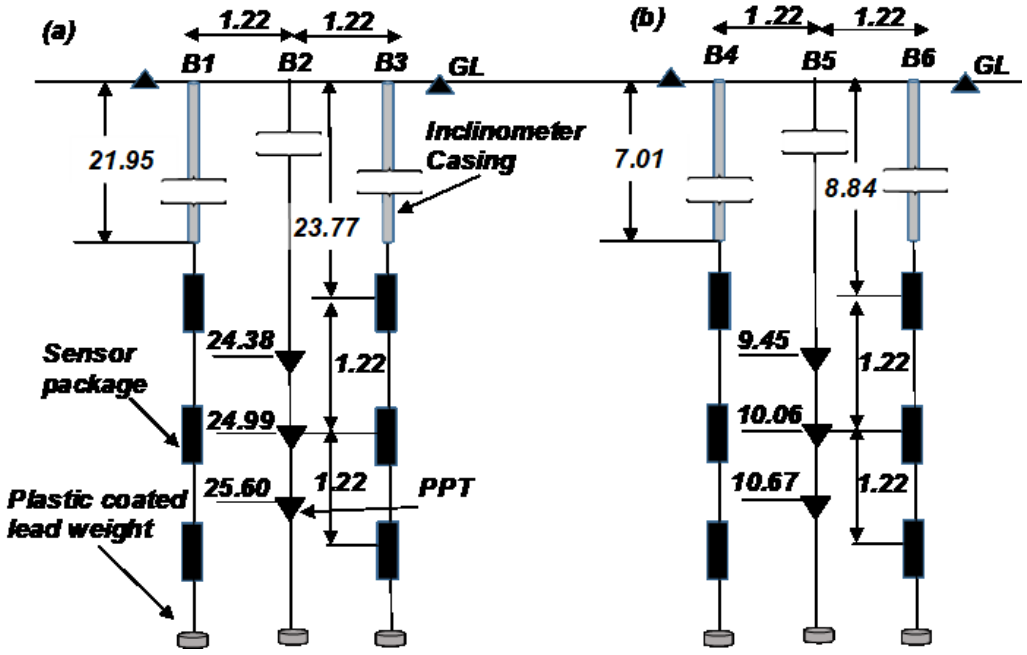

Figure 3.1. Elevation view of the planned (a) deep sensor array, and (b) shallow sensor array. For clarity, boreholes housing inclinometer casing with sondex rings and surface sensors are not shown here. All dimensions shown are in meters (1 m = 3.2808 ft.).

In order to measure pressure consistently and accurately, the housing and PPT must be de-aired. The procedures followed to prevent air bubbles from entering the PPT housing consisted of the following: first, the porous bronze filters were boiled for 10 minutes before installation into the housing in order to remove air bubbles. Then, each PPT housing was assembled underwater and each PPT was de-aired by placing a small object into its diaphragm chamber and removing entrapped air bubbles. Thereafter, a water tight membrane was placed over the PPT before removing the PPT housing from the water, and removed once the PPT was placed into service. PPTs used to monitor pore pressure within the silt layer were installed within borehole B-5 (Figure 2.1) and grouted in accordance with procedures recommended by Mikkelsen and Green (2003).

3.2.2 Calibration Protocols

The PPTs were calibrated located at the Geotechnical Engineering Field Research Site (GEFRS) at OSU. Each instrument was placed at the bottom of a water-filled 19.8 m long inclinometer casing and raised in intervals of 1.5 m. At each measurement location, the PPT was fixed in place for approximately 30 seconds while the excitation voltage was measured at a sampling rate of 50 Hz (Figure 3.3a). Owing to the full gain setting of 5 V set in consideration of the application to observing blast-induced pressures (which were anticipated to be large based on previous studies [e.g., Gianella and Stuedlein 2017]), the noise in the excitation voltage varied by $1.5E^{-3}$ mV. Thus, an average value hydrostatic pressure was calculated from the ~1,500 readings taken over the 30 second period to provide a representative magnitude for the purposes of calibration. Calibrations from the factory and these analysis also differ, verifying the need for custom calibrations. Figure 3.3a illustrates that the maximum and minimum amplitudes were 0.18 mv and $6E^{-3}$ mV which occurred at the depths of 19.8 m and 1.5 m, respectively. These corresponds to the hydrostatic pressures of 15 kPa and 194.4 kPa as shown in Figure 3.3b. The factory and custom calibration factors for each PPT are presented in Table 3.1.

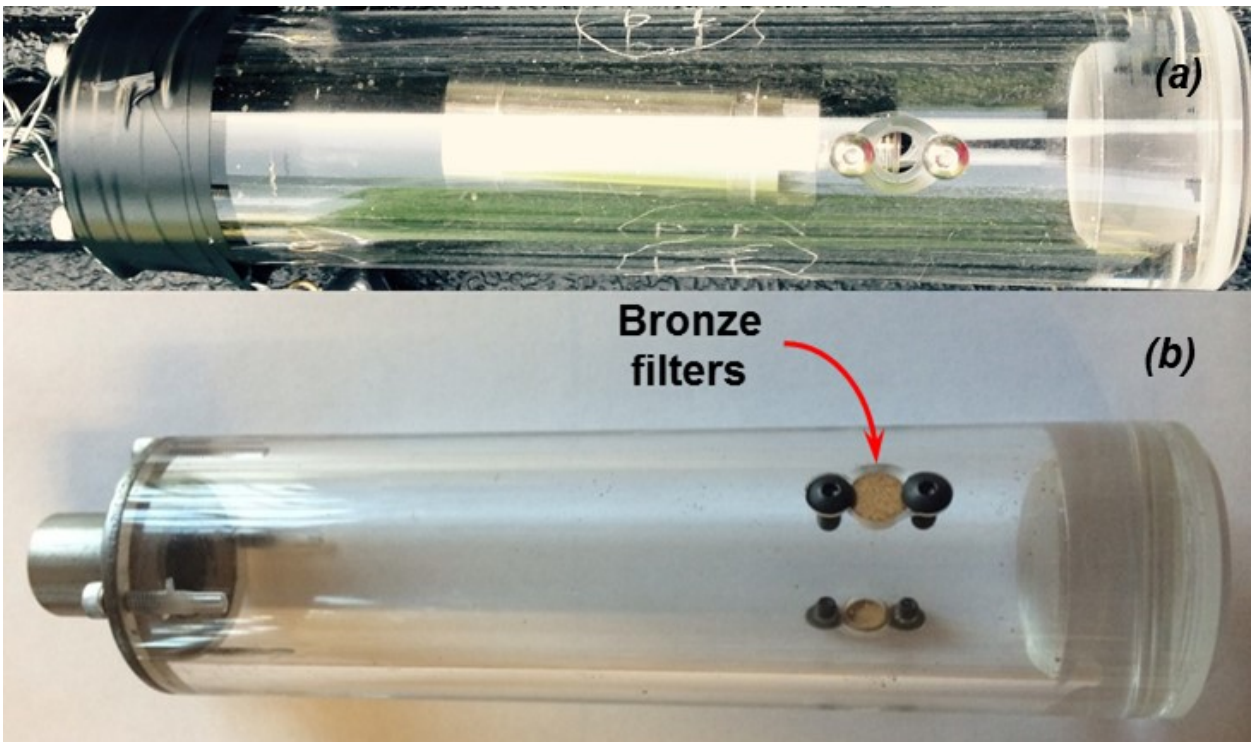

Figure 3.2. Photographs showing the PPT housing: (a) PPT placed in the PPT housing with the PPT diaphragm chamber aligned with the location of porous bronze filters, and (b) with porous bronze filters shown.

Table 3.1. Comparison of Calibration Factors Determined in the Field to those Reported by the Manufacturer.

PPT	Factory Calibration (Excitation, *V* to Pressure, *u* (kPa))	Calibration Equation (Excitation, *V* to Pressure, *u* (kPa))	Coefficient of Determination, R^2
1	u=1033.8005 V-5.1690	u =1041.2557 V+10.1946	0.99999
2	u=1034.2140 V-7.2394	u =1039.9900 V +8.2572	0.99999
3	u= 1034.6279 V -7.2424	u =1041.0373 V +8.6863	0.99999
4	u= 1034.0071 V +23.7822	u =1039.0437 V +13.2819	0.99999
5	u= 1038.6005 V -6.2028	u =1042.2058 V +8.8506	0.99999
6	u=1034.8349 V+5.1742	u =1040.2892 V +16.6266	0.99983

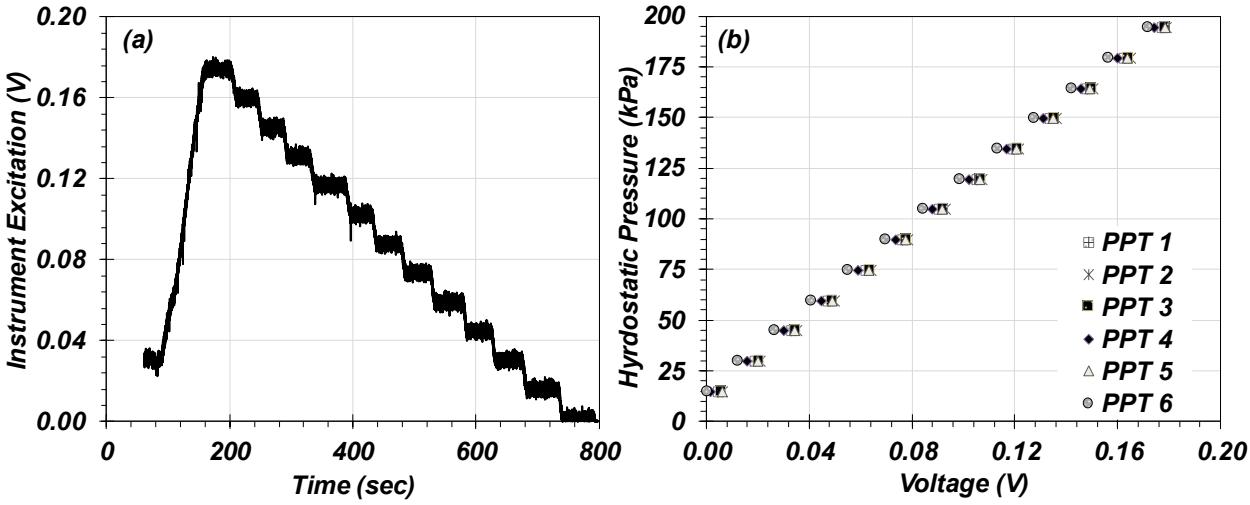

Figure 3.3. Pore pressure transducer (PPT) calibrations, including: (a) step function illustrating pore pressure at the different depths inside the inclinometer casing, and (b) the variation in voltage measured and corresponding pore pressure for each PPT

3.3 BLASTING PROGRAM

Excess pore pressures were raised within the silt layer through the use of explosives. Selection of the charge weights and detonation sequence was based on variety of factors governing the suite of overall project objectives driven by the Port of Portland. The objectives included:

- Evaluation of the threshold shear strain to produce soil nonlinearity;
- Evaluation of the threshold shear stain to produce excess pore pressures;
- Development of the relationship between shear strain and shear modulus degradation;
- Development of the relationship between shear strain and excess pore pressure generation;

- Evaluation of the magnitude of vertical strain and overall ground surface settlement as a result of dissipation of excess pore pressures; and,

- Rate of shear modulus recovery with dissipation of excess pore pressures.

These objectives led to the selection of a charge weight distribution that initiated with small charges located at a great distance from the instrumented array, increased to a maximum charge weight at intermediate distances, and followed by a reduction in charge weight as the distance between the charges and the array decreased to a minimum. The explosives and detonation system consisted of Pentex cast boosters with iKon electronic detonators and Cordtex TDS detonation cord. Three decks of charges were placed within each of the ten blast casings to produce a blast sequence of 30 individual charges. Table 3.2 indicates each charge position as high (H; the uppermost charge within the blast casing), intermediate (M; the middle charge), and low (L; the lowest or deepest charge in the blast casing). Charge weights ranged from 90 to 1,814 grams and were detonated over a duration of 30 seconds in the sequence and depth as shown in Table 3.2 and Figure 3.4, below. Figure 3.5 provides a graphical representation of the charge weight and detonation time history.

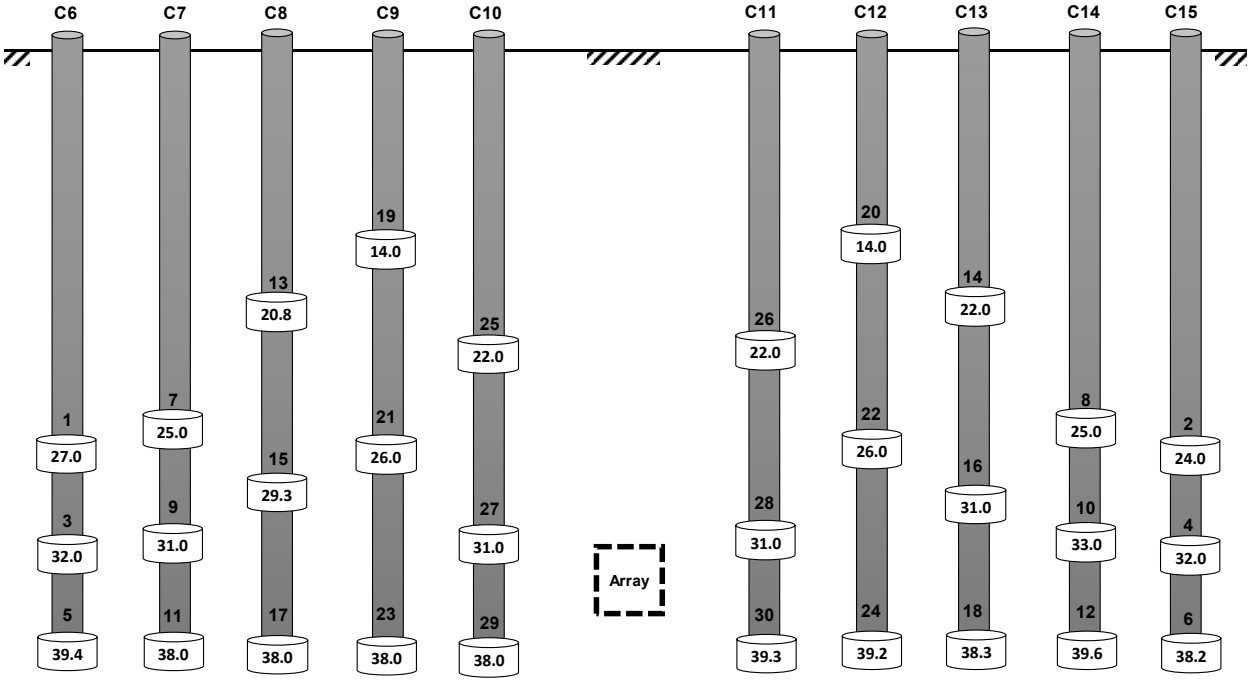

Figure 3.4. Schematic indicating bottom depth of charge (in feet) and charge number for explosives distributed within blast casings C6 through C10 (Side A, compare to Figure 3.5) and C11 through C15 (Side B).

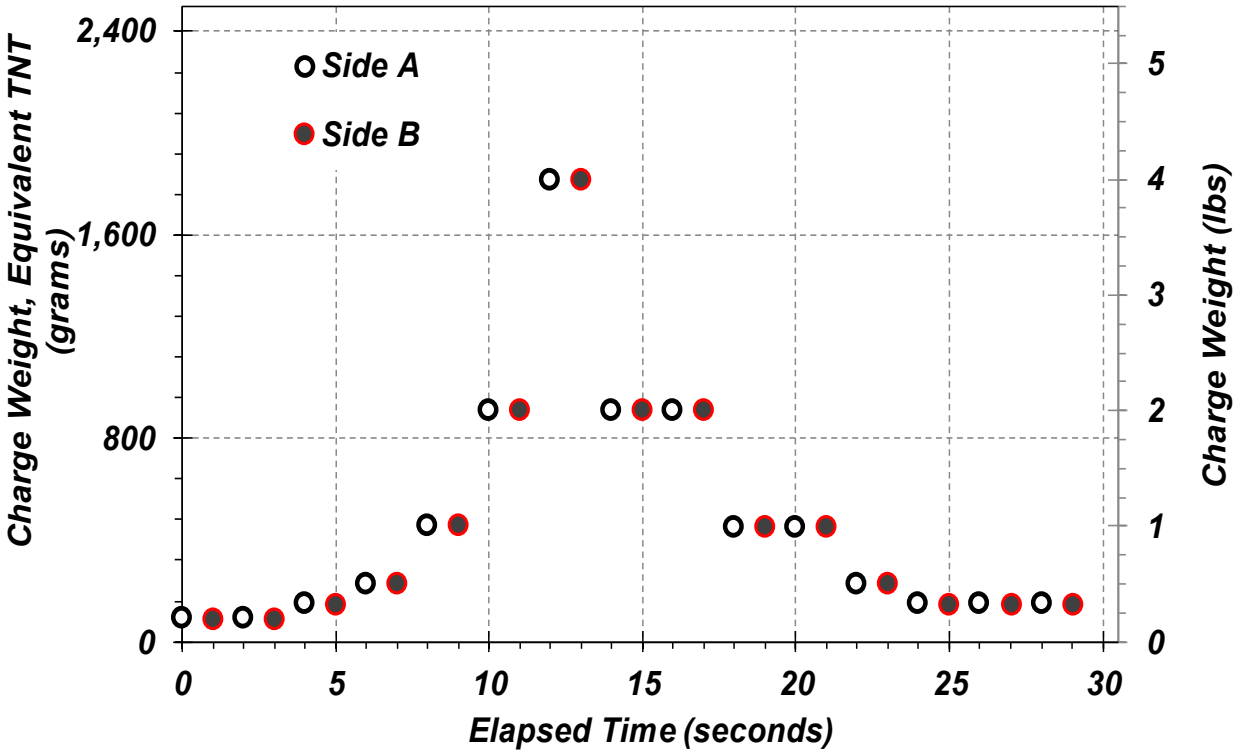

Figure 3.5. Schematic indicating bottom depth of charge (in feet) and charge number for explosives distributed within blast casings C6 through C15

Table 3.2. Schedule of Charge Detonations for the Shallow Instrumented Array within the Silt Layer.

Charge number	Charge position	Actual bottom of charge (ft.)	Blast Casing Number	Time (ms)	Charge weight equivalent TNT (lbs.)	Charge Weight, Equivalent TNT (g)
1	H	27.00	C6	500	0.20	90.72
2	H	24.00	C15	1,500	0.20	90.72
3	M	32.00	C6	2,500	0.20	90.72
4	M	32.00	C15	3,500	0.20	90.72
5	L	39.42	C6	4,500	0.33	149.68
6	L	38.17	C15	5,500	0.33	149.68
7	H	25.00	C7	6,500	0.50	226.80
8	H	25.00	C14	7,500	0.50	226.80
9	M	31.00	C7	8,500	1.01	458.13
10	M	33.00	C14	9,500	1.01	458.13
11	L	38.00	C7	10,500	2.01	911.72
12	L	39.58	C14	11,500	2.01	911.72
13	H	20.75	C8	12,500	4.00	1814.36
14	H	22.00	C13	13,500	4.00	1814.36
15	M	29.33	C8	14,500	2.00	907.18
16	M	31.00	C13	15,500	2.00	907.18
17	L	38.00	C8	16,500	2.00	907.18
18	L	38.33	C13	17,500	2.00	907.18
19	H	14.00	C9	18,500	1.00	453.59
20	H	14.00	C12	19,500	1.00	453.59
21	M	26.00	C9	20,500	1.00	453.59
22	M	26.00	C12	21,500	1.00	453.59
23	L	38.00	C9	22,500	0.50	226.80
24	L	39.17	C12	23,500	0.50	226.80
25	H	22.00	C10	24,500	0.33	149.68
26	H	22.00	C11	25,500	0.33	149.68
27	M	31.00	C10	26,500	0.33	149.68
28	M	31.00	C11	27,500	0.33	149.68
29	L	38.00	C10	28,500	0.33	149.68
30	L	39.33	C11	29,500	0.33	149.68

3.4 VANE SHEAR TEST AND PROTOCOLS

The undrained shear strength of plastic soils of very soft to medium stiff consistency is commonly evaluated using the vane shear test (VST). The test is generally conducted by drilling a borehole to the desired elevation, inserting a four-bladed vane (Figure 3.6) into the base of the prepared borehole to a depth of 200 mm (8 inches) in a single, smooth thrust, and then applying torque to the connecting rods at the ground surface to twist the vane and thus shear the soil. The torque is measured using a calibrated torque wrench (Figure 3.7). Rotation of the vane generates a cylindrical shearing surface, and the torque used to shear the vane is converted to the equivalent shearing resistance through consideration of limit equilibrium analyses. The vane shear testing was conducted in general accordance with ASTM D 2573 (ASTM 2019), although some modifications were selected by the technician performing the test based on his experience. One of the benefits of the VST is that the test method allows the determination of both the peak and residual undrained shear strength: the rate of rotation to observe the maximum torque is relative slow (about 6 degrees per minute), thereafter, the vane is rotated very quickly to remold the soil and the residual torque necessary to rotate the vane is measured, giving an indication of the residual undrained shear strength. When performed in a borehole that provides direct access to the test depth, there is no significant effect of rod friction due to exposure of the rod to a negligible length of soil. However, rod friction can be significant when the VST is conducted in the absence of prepared depths, and the measurement of friction of the rods without a vane attachment is necessary in order to correct for the friction effect.

Several assumptions are required to calculate the undrained shear strength measured from the VST, including (Kulhawy and Mayne 1990):

- The soil responds in an undrained manner during shearing, and no dissipation of pore pressure generated due insertion and rotation of the vane occurs;
- The act of drilling and inserting the vane does not result in disturbance of the soils;
- The act of drilling and inserting the vane does not result in disturbance of the soils;
- The zone of remolded soil surrounding the vane following insertion is negligible in extent and effect;
- The rotation of the vane causes simultaneous failure along the entire cylindrical failure surface (i.e., progressive failure does not occur); and,
- The soil does not exhibit significant anisotropy (i.e., all soil properties are equal in all directions).

In general, the assumption of undrained shearing behavior is generally met for soils with significant plasticity, such as those silt soils that form the target soils at the test site. The use of mud-rotary drilling ensures that a minimal amount of disturbance occurs at the base of the borehole. However, the magnitude of disturbance associated with vane insertion is unknown. During shearing, it is likely that progressive failure does occur but is a function of vane size: the smaller vane used in this study (described below) should limit the effects of progressive failure.

Finally, the assumption of soil isotropy is unlikely to be met due to the typical one-dimensional deposition process of alluvial soils.

Figure 3.6. Photograph showing Vanes A, B, and C evaluated in the field for determination of the undrained shear strength.

Owing to the relationship between the strength of the soil and the torque mobilized during the VST, several sizes of vane are available to accommodate the range in undrained shear strength that a soil may exhibit. The tests conducted at the PDX test site initiated with the largest vane (Vane C, Figure 3.6) and at the shallowest depths (discussed in detail in Section 4), but could not be rotated due to the relatively high strength of the soil at that location. The second vane shear test attempted used Vane B; however, this vane was too large relative to the strength of the soil and so the test was aborted. All remaining tests were successfully conducted using Vane A, which is characterized with:

- length of 89 mm (3.5 inches);
- height of 51 mm (2 inches);
- vane blade thickness of 2 mm (0.08 inches);
- shaft diameter of 19 mm (0.76 inches); and,
- vane area ratio of 0.17.

Figure 3.7. Photograph showing the scale used to measure torque mobilized by the vane (photo shows pre-rotation null torque).

Calculations of undrained shear strength as deduced from the measured torque, T (in N-m), followed the ASTM standard (ASTM 2019). The field vane-measured undrained shear strength, $s_{u,fv}$ (in kPa), for tapered vanes is computed using:

$$s_{u,fv} = \frac{12 \cdot T \cdot K}{\pi D^2 \cdot \left(\frac{D}{\cos i_T} + \frac{D}{\cos i_B} + 6H\right)} \quad \textbf{(3-1)}$$

where:

D = vane diameter (in mm),

H = height of the vane (in mm),

K = a constant, equal to $1x10^6$, and

i_T and i_B equal the angle of taper for the vane top and bottom, respectively, with both equal to 45°.

The calculation of the field vane-measured residual undrained shear strength, $s_{ur,fv}$, uses the same approach (i.e., Eq. (3-1)). The potential for strength loss possible in plastic soils subject to large shear strains is commonly described using the sensitivity, S_T, of the soil, given by:

$$s_{T,fv} = \frac{s_{u,fv}}{s_{ur,fv}}$$

(3-2)

Which expresses the sensitivity as a ratio of the peak and residual undrained strengths. Generally speaking, the higher the magnitude of S_T, the greater the potential for rapid strength loss due to shearing. Table 3.3 provides typical values of sensitivity as a function of region of interest.

Table 3.3. Typical Qualification for Sensitivity of Plastic Soils Based on Region (after Holtz et al. 2011).

Condition	Range of Sensitivity, S_T		
	U.S.A.	**Canada**	**Sweden**
Low Sensitive	2 – 4	< 2	< 10
Medium Sensitive	4 – 8	2 – 4	10 – 30
High Sensitive	8 – 16	4 – 8	> 30
Extra Sensitive	–	8 – 16	> 50
Quick	–	> 16	> 100

The undrained shear strength measured with a field vane is subject to viscous effects, such that strength of the soil increases as the rate of vane rotation increases (Chandler 1988). The viscous effect varies with the plasticity of the soil and can be corrected using a correction factor, C_{fv}:

$$C_{fv} = 1.05 - b(PI)^{\frac{1}{2}}$$

(3-3)

where:

PI is the plasticity index, and

b is a constant that varies with the time to failure, t_f:

$$b = 0.015 - 0.0075 \log t_f$$

(3-4)

The corrected undrained shear strength is then computed using:

$$s_u = C_{fv} \cdot s_{u,fv}$$

(3-5)

4.0 RESULTS OF THE TEST PROGRAM

The scope of this investigation included the evaluation of the initial, *in situ* undrained shear strength of the silt layer, the execution of a controlled blast-liquefaction experiment, and the measurement of post-blast undrained shear strength of the silt layer. The initial undrained shear strength, as characterized using the VST, was conducted on 19 June 2018. The controlled blasting of the silt layer was conducted on 5 October 2018, with the post-blast VSTs conducted immediately thereafter on the same day. The following subsections of this report describe the results of these three research activities.

4.1 INITIAL *IN SITU* VANE SHEAR STRENGTH

Vane shear strength tests were conducted within borehole V-1 by a representative of In Situ Engineering with drilling support by Holt Services, Inc. Following the aborted attempts in conducting VSTs with Vane B and C, successful VSTs were performed using Vane A and initiating within VST-1 at a depth of 9.0 m (29.5 ft.; Table 4.1). Following VST-1, the drilling crew resumed mud-rotary drilling to the next depth and VST-2 conducted. As indicated in Table 4.1, depth increments ranged from 0.3 to 0.6 m (1 to 2 ft.), smaller than the typical 0.76 m (2.5 ft.), in order to obtain strength measurements on as high of a resolution as possible without imposing on the quality of the test data. The corrected peak undrained shear strength of the silt layer was observed to vary between 58 and 158 kPa (1,210 and 3,300 psf), representative of medium stiff to very stiff consistency. Based on the residual undrained shear strength measurements and Table 3.3, the silt layer exhibited "low" sensitivity, indicating that the potential for large quasi-static deformations is low.

Figure 4.1 compares the strain-rate effect corrected peak and residual undrained shear strength measured in borehole V-1 to the corrected cone tip resistance, q_t, for CPT-3 measured over the same depth interval. For reference, borehole V-1 was located 3.9 m (12.7 ft.) northwest of CPT-3 (refer Figure 2.1). Figure 4.1 shows that: (1) there is a clear correspondence between q_t and s_u, and (2) $s_{u,r}$ exhibits an apparent and commonly-observed linear trend with depth. It is of interest to compare the field vane results to laboratory strength tests: consolidated undrained triaxial compression and monotonic direct simple shear tests returned undrained shear strengths of approximately 62 kPa (1,300 psf) and 50 to 60 kPa (1,040 to 1,250 psf), respectively, for specimens prepared from similar depths as the VSTs. These laboratory tests appear to confirm the lower-bound magnitudes of corrected s_u measured using the VST.

Due to the availability of CPT rigs for subsurface investigation in the state of Oregon, the development of a correlation between the VST results and more common CPT corrected cone tip resistance, q_t, was deemed of interest. The correlation between q_t and s_u is frequently investigated using the cone factor, N_k, given by

$$\boldsymbol{s_u = (q_t - \sigma_{vo})/N_k}$$

(4-1)

where:

σ_{vo} = the total vertical stress at the elevation of the VST and

q_t measurement.

Figure 4.2 presents the back-calculated values of the cone factor with depth; in general, N_k = 10 and 22 appears to capture the peak and residual undrained shear strength of the silt layer investigated.

Table 4.1. Vane Shear Test results for Peak and Residual Shear Strength

Vane Shear Test No.	Depth (m/[ft])	Peak undrained shear strength, $s_{u,fv}$ (kPa/[psf])	Residual undrained shear strength, $s_{ur,fv}$ (kPa/[psf])	Representative plastic index, *PI*	Corrected peak undrained shear strength, s_u (kPa/[psf])	Corrected residual undrained shear strength, s_{ur} (kPa/[psf])	Sensitivity, S_T
1	9.00 [29.53]	89 [1,860]	30 [630]	26	87 [1,820]	29 [610]	3.0
2	9.30 [30.51]	59 [1,230]	30 [630]	26	58 [1,210]	29 [610]	2.0
3	9.76 [32.02]	98 [2,050]	39 [820]	26	95 [1,990]	38 [790]	2.5
4	10.20 [33.46]	74 [1,550]	39 [820]	26	72 [1,500]	38 [790]	1.9
5	10.70 [35.10]	62 [1,300]	36 [750]	30	60 [1,250]	38 [790]	1.6
6	11.10 [36.42]	95 [1,990]	42 [880]	30	92 [1,920]	40 [840]	2.3
7	11.70 [38.39]	163 [3,410]	42 [880]	30	158 [3,300]	40 [840]	3.9

4.2 PORE PRESSURE RESPONSE TO BLASTING

Detonation of the 30 second blasting sequence was conducted at approximately 11:58 AM on 5 October 2018. The pore pressure response to the controlled blasting program was immediately apparent as measured using the PPTs, with clear distinction between the primary wave (*p*-wave) induced pore pressure (peak hydrodynamic high-frequency pulse) and the low frequency shear wave (*s*-wave) induced pore pressure. Figure 4.3a presents the excess pore pressure time history over the full range of measured pore pressures during and immediately after the blast sequence, whereas Figure 4.3b presents the same data but over a smaller range in pore pressure and in terms of the excess pore pressure ratio, r_u, given by:

$$r_u = \frac{u_e}{\sigma'_{v0}} \tag{4-2}$$

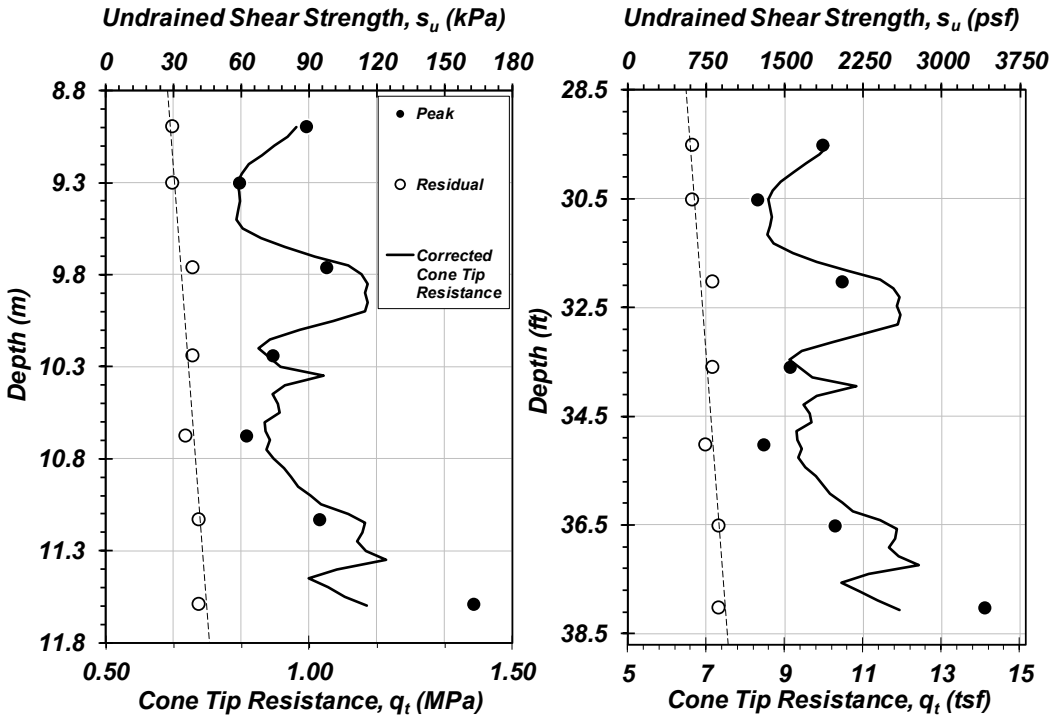

Figure 4.1. Comparison of peak and residual undrained shear strength measured at borehole V-1 with depth to the corrected cone tip resistance observed at CPT-3: (left) metric units, and (right) imperial units

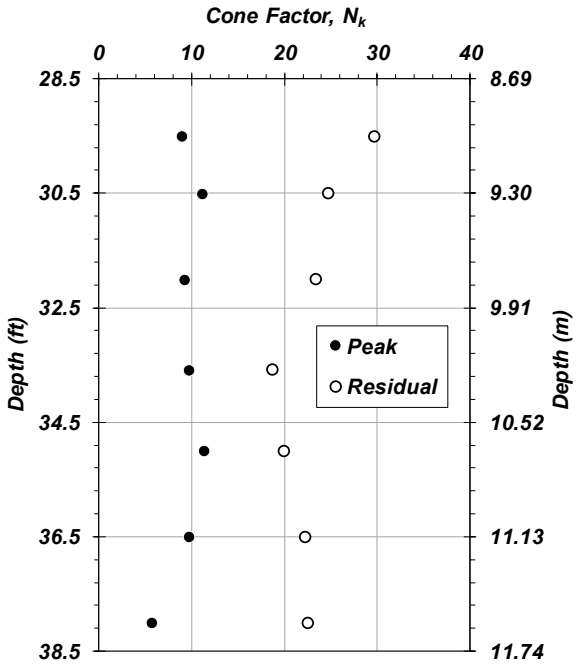

Figure 4.2. Back-calculated cone factors for use in forward estimation of peak and residual undrained shear strength for the silt layer investigated.

where:

u_e = excess pore pressure,

σ'_{v0} = the initial vertical effective stress at the depth of each PPT.

For reference, the depths of the PPTs are 9.50, 10.00, and 10.67 m (31.17, 32.8, and 35 ft.) for PPT 3, PPT 5, and PPT 2, respectively.

The excess pore pressure ratio simply scales those pore pressures in excess of hydrostatic pore pressure, where a r_u = 0% and 100% indicate hydrostatic and liquefied (zero effective stress) conditions. Note that although the magnitude of excess pore pressure is an indication of liquefaction, the duration of sustained excess pore pressure is of as much or greater importance with respect to the consequences of liquefaction.

As shown in Figure 4.3a, the peak *p*-wave-induced pore pressure reached a maximum of about 415 kPa, equal to approximately r_u = 800%, or indicating a state of instantaneous and ephemeral liquefaction in terms of the excess pore pressure ratio. Inspection of the frequency response of the particle velocities measured using the TGPs and PPTs indicates that the *p*-wave pore pressure pulse operated at dominant frequencies on the order of 300 to 500 Hz (corresponding to 2 to 3 milliseconds). In general, controlled blasting is conducted to raise the *residual* excess pore pressures (Gianella and Stuedlein 2017), or those excess pore pressures that result from passage of shear waves and persist following each blast pulse. Figure 4.3b presents more clearly the magnitude of the peak residual excess pore pressures generated in the silt layer, corresponding to r_u of 12.6 to 17.5% (note that Figure 4.3b obscures the true peak residual excess pore pressure

due to the scale of the figure). Thus, sustained liquefaction, defined as r_u = 100%, was not achieved in the silt layer, and so the focus of the investigation shifts to the phenomenon of cyclic softening of this layer. The magnitude of r_u generated is indicative of the degree of plasticity of the silt layer as indicated by the laboratory test data derived by Oregon State University and described in Section 2.2. Furthermore, these pore pressures indicate that this silt layer responds in a more "clay-like" material (Idriss and Boulanger 2006) than "sand-like", due to the magnitude of PI of the silt.

Figure 4.4 presents the dissipation time history of the blast-induced excess pore pressure ratios to aid the interpretation of the post-blast VSTs. Note that due to acquisition noise and the high sampling rate (10 kHz), the data shown in Figure 4.4 has been smoothed and down-sampled to 0.1 Hz to facilitate appropriate presentation of the results. Accordingly, the blast pulse-induced excess pore pressure shown in Figure 4.3 are not represented in Figure 4.4. As indicated, the peak residual excess pore pressures persisted within the silt layer for approximately 20 to 40 minutes prior to dissipating. The excess pore pressures at the depth of PPT 5 (depth of 10.00 m or 32.8 ft.) dissipated to zero at approximately 4,400 minutes (3 days), whereas PPTs 2 and 3 indicated that zero excess pore pressure was achieved at approximately 11,400 minutes (8 days). This information is critical for anticipating instability, and determining the potential for large, post-earthquake deformations, of geotechnical structures (e.g., retaining walls, abutments and approach fills, natural and cut slopes, etc.). The range in time corresponding to the conduct of VSTs is shown in Figure 4.4 for reference to the results in Section 4.3, and indicates that the excess pore pressures remained relatively constant over this period. Note that the gaps in acquired data present in Figure 4.4 are due to occasional periods of lack of fuel for the generator powering the data acquisition system.

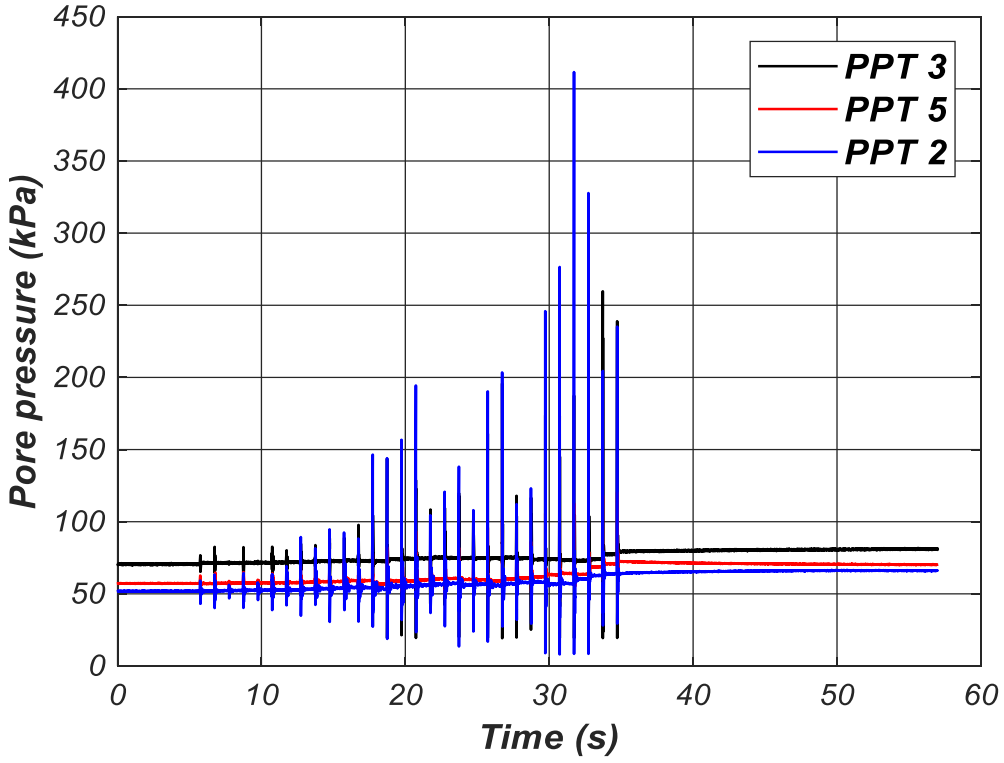

(a)

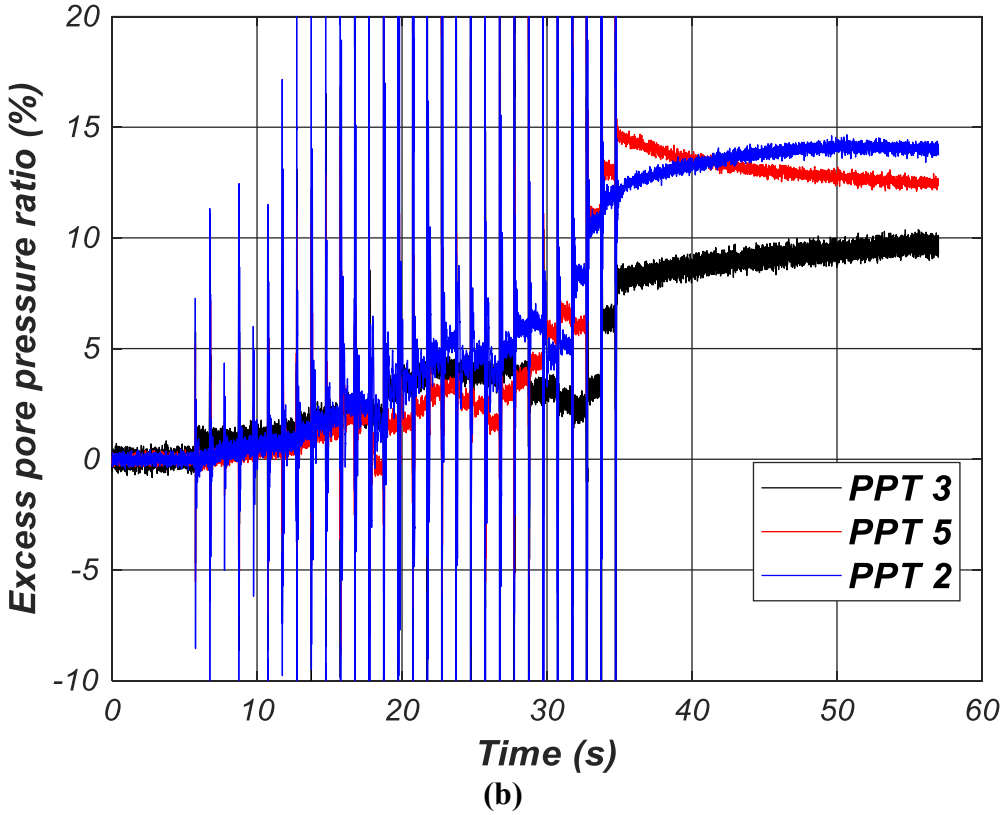

(b)

Figure 4.3. Pore pressure response to blast program (a) measured pore pressure time history, and (b) excess pore pressure ratio time history

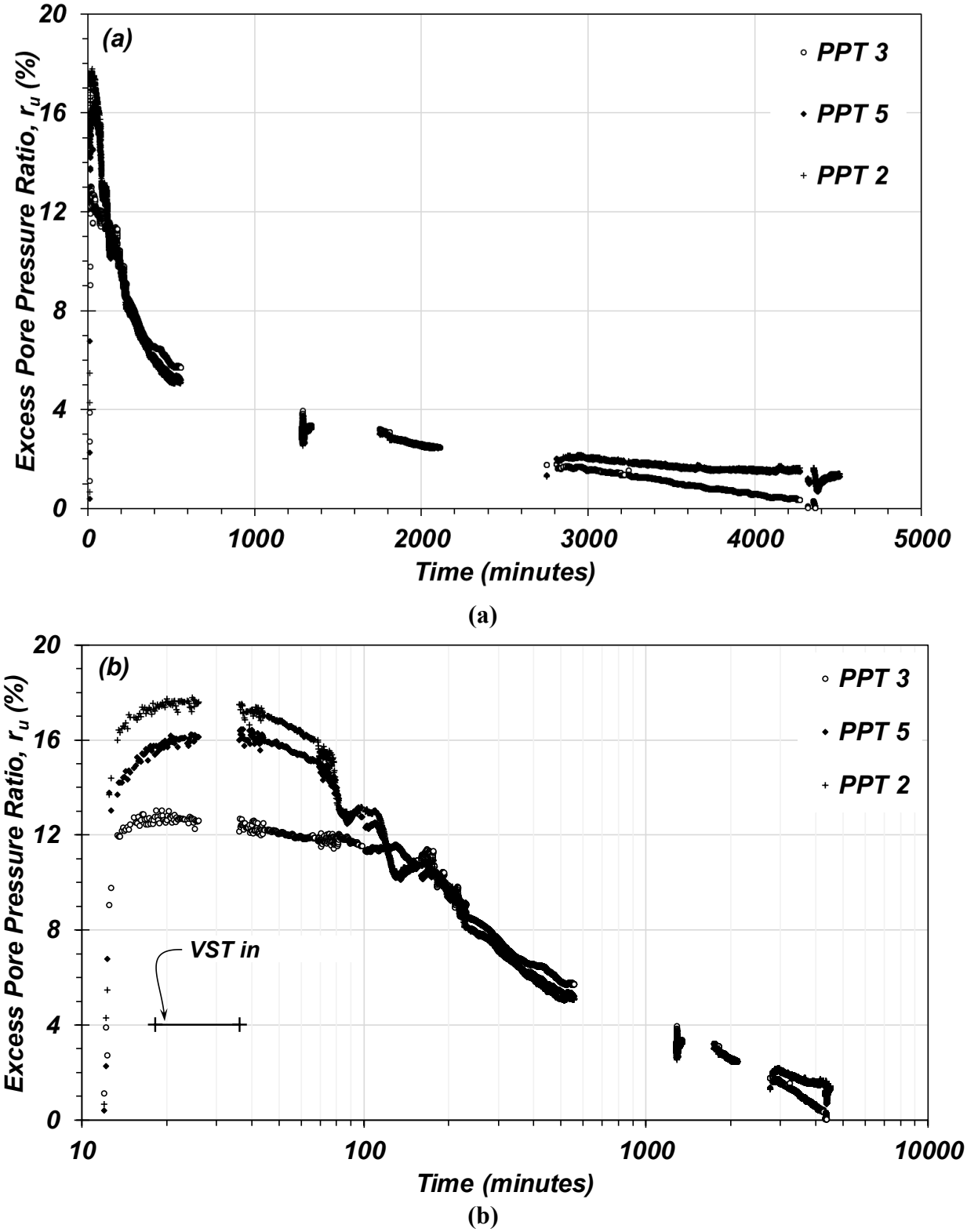

Figure 4.4. Dissipation time history of blast-induced pore pressures as observed in the silt layer: (a) arithmetic scale, (b) semi-logarithmic scale. Note that $t = 0$ at 11:47:46.744771 AM on 5 October 2018.

4.3 POST-BLAST VANE SHEAR STRENGTH

4.3.1 Experimental Setup

Special arrangements were necessary to accommodate VSTs immediately after the 30 second blast sequence. Due to the complexity of the blast experiment and duration required to drill and conduct each VST test (approximately two to three hours), it was considered too risky and otherwise infeasible to place a drilling rig and crew on standby to conduct the VSTs. Examination of Figure 4.4 shows that the risk of missing peak excess pore pressures during vane shear testing would have been realized, and that the judgment of this risk during experiment planning was correct.

Based on the assumed risk of missing the window of time necessary to conduct the VSTs, an access casing was installed prior to the blast experiment and concurrent with instrument installation. The access casing was installed within a 200 mm (8 inch) diameter mud-rotary borehole V-2 (Figure 2.1), located 1.2 m (4 ft) south of PPT string of borehole B-5, and advanced to a depth of approximately 9 m (30 ft). The access casing installed within borehole V-2 consisted of an open-ended 150 mm (6 inch) PVC casing. Following placement of the casing, the drilling fluid in the casing was flushed with water to a depth of 6 m (20 ft) to remove a significant portion of the highly-plastic drilling mud. The intent was to leave a portion of the mud in the casing to settle out and provide a hydraulic seal between the water above, and the silt soil below, the access casing. It appears that lack of full removal of the drilling mud resulted in an adverse effect on some of the VST results, as described below.

Prior to the blast experiment, a skid rig delivered to the site by In Situ Engineering was pre-positioned over borehole V-2 as shown in Figures 4.5 and 4.6. Sand bags placed on the skid rig were used to provide weight and coupling to the ground in anticipation of large nearfield blast-induced vibrations. CPT rods 8 m (27 ft) in length and used to extend the vane to depth were suspended from the skid rig to allow quick extension and immediate shear testing following the post-blast all-clear. Figure 4.7 presents photographs of the skid rig-facilitated VSTs following blasting and conducted using a manually-operated torque wrench. The time of each VST was noted and synchronized to the data acquisition system monitoring excess pore pressures for interpretation of potential strength loss, as discussed in Section 4.3.2, below.

Figure 4.5. Weighted skid rig pre-positioned over borehole V-2 with 8 m (27 ft.) of CPT rod and VST attachment suspended over the base of the borehole just prior to the 30 second blast experiment.

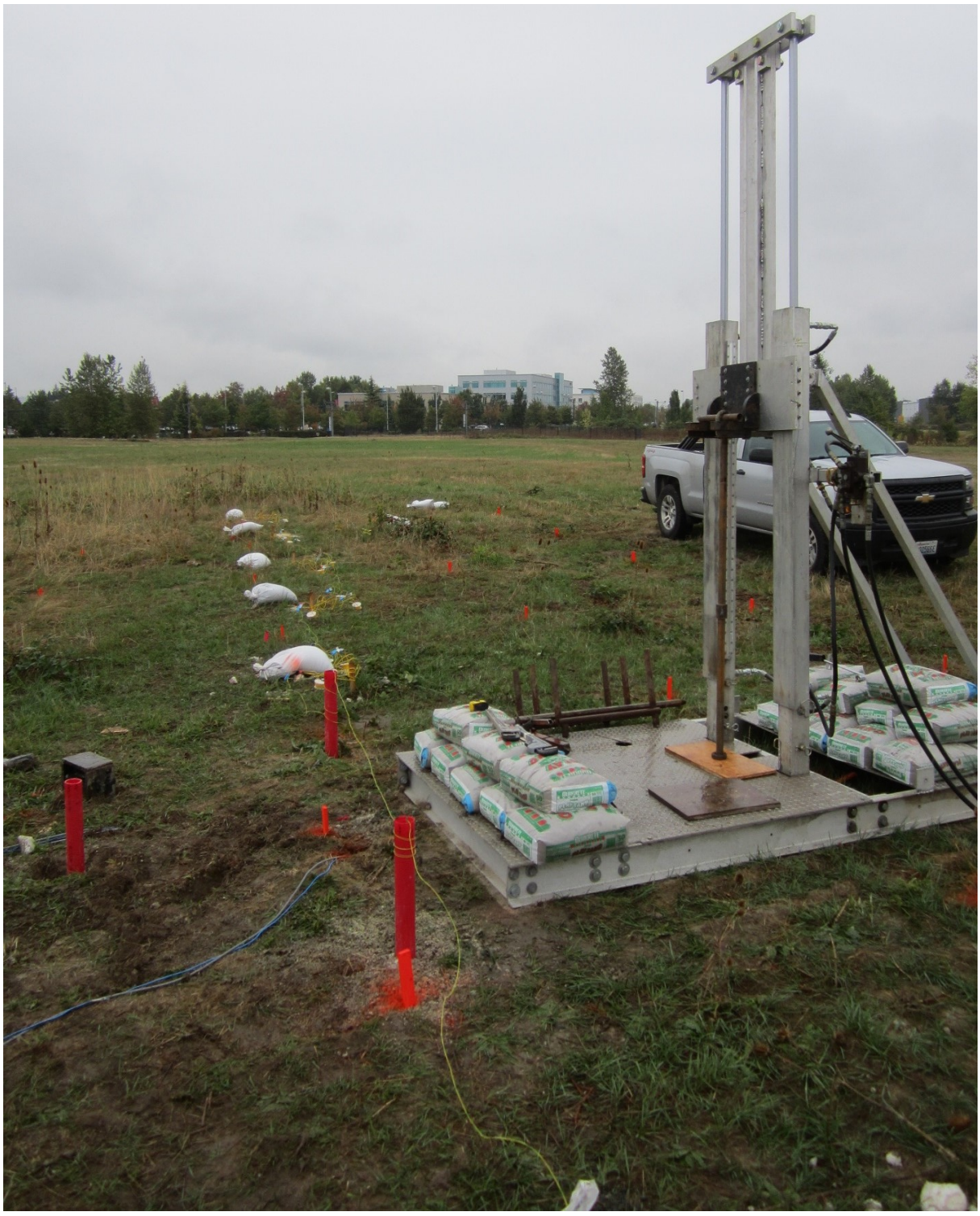

Figure 4.6. View of weighted skid rig pre-positioned over borehole V-2 just prior to the 30 second blast experiment, looking east to show blast casings loaded and weighted with sand bags along the east-west array alignment (compare to Figure 1).

Figure 4.7. Photographs of post-blast VSTs in progress with manually-operated torque wrench. Each VST was observed and time noted in synchronization with the data acquisition system used to monitor the excess pore pressures.

4.3.2 Vane Shear Test Results

Upon the declaration of the all-clear by the licensed blaster following the 30 second blast experiment, a representative of In Situ Engineering initiated the vane shear testing with assistance by members of the research team. The vane (Vane A; see Section 3.4) was inserted to depth of a 9.64 m (31.64 ft) into the soil below the base of the access casing using the skid rig and sheared to produce the peak and residual undrained shear strength. Thereafter, the vane was pushed to the next depth and the process repeated to result in six VSTs following blasting. The time between each VST was approximately 3 minutes on average, to result in a total duration of testing of about 18 minutes. Following the 2nd test, increasing difficulty in performing the VST was noted. Two possible contributors to increased torque to shear the soil were identified: (1) increasing rod friction generated along the circumferential area of the cone rods used to deliver the vane to the test depth, and (2) the presence of heavy, thixotropic, bentonite-rich drilling fluid suspended above the base of the borehole into the silt layer along the annulus between the cone rods and the adjacent soil contributed significant shearing resistance. Following the VST program, the cone rods and vane were retrieved from the borehole to remove the vane and evaluate the magnitude of rod friction in the silt layer. The rods (without vane) were re-inserted into the borehole to a depth of 1.3 m (4.28 ft) and torqued to observe the peak and residual shearing resistance. This enabled corrections to the vane shear tests where thixotropic effects were not suspected.

The rod friction correction was conducted within an accepted mechanical framework as follows. The peak and residual torque measured over the length of the inserted rod was measured equal to 63.7 N-m (47 ft.-lbs.) and 47.5 N-m (35 ft.-lbs.), respectively. The torque per unit length is then calculated by dividing the measured torque by the length of rods within the silt layer, resulting in unit torque magnitudes of 14.9 N-m/m (11 ft.-lbs./ft.) and 11.1 N-m/m (8.2 ft.-lbs./ft.). To correct the measured torque for rod friction, the length of rod used for each VST is multiplied by the unit rod friction torque and subtracted from the measured torque, with peak and residual torques applied to each relevant portion of the length of rod. This correction was applied to each of the six test depths.

The second suspected contributor to increased torque is hypothesized to result from thixotropic shear of the bentonite/silt interface or swelling of the clay minerals within the silt upon interaction with the bentonite fluid. Thixotropic fluids, such as hydrated bentonite drilling fluid that has sedimented into a thick viscous fluid can result in significant shearing resistance in dynamic environments. Thixotropic fluids exhibit a shearing resistance that increases with the shear strain rate applied. As the cone rods are rapidly torqued to fail the silt soil, the corresponding shear strain rate increases to result in an increasing fluid shearing resistance that would manifest as an increasing torque measured at the ground surface. This effect could have been exacerbated by swelling of the clay minerals within the silt layer as the drilling fluid and water flowed along the cone rods to hydrate the silt layer. Since hydration of clay minerals is a time-dependent process, the longer the silt layer was in contact with foreign fluids, the greater the potential for increased swell pressures to act on the cone rods. Unfortunately, there is no simple or otherwise possible correction with the information available to account for the magnitude of increased torque associated with thixotropy of the bentonite drilling fluid or swelling of the silt layer.

The first and second VST was conducted within the first 4.5 minutes of testing. The calculated rod friction for these two tests was smaller than the measured torque, as expected in the absence of thixotropic/swelling effects, and the measured torque could be reliably corrected for rod friction. However, the rod friction magnitude was calculated to be equal to or larger than the measured torque for the third through the sixth test, and the undrained shear strength could not be reliably determined. It is noted that the sixth VST required significant effort to advance the vane to the test depth (12.14 m or 39.84 ft) and to rotate the vane; the test depth corresponded to the known contact with the underlying sand layer and therefore, the sixth VST could not be admitted for evaluation of the undrained shear strength on that basis.

Table 4.2 presents the vane shear test results following blast-liquefaction corrected for shear strain rates and rod friction. As shown, only the first two VSTs could be reliably interpreted. The peak undrained shear strength for the first and second VSTs was 39.3 and 37.8 kPa (821 and 791 psf), respectively. Table 4.3 and Figure 4.8 compares the peak and residual post-blast undrained shear strength for the silt layer to the initial undrained shear strength measured in borehole V-1. For the purposes of comparison of undrained shear strengths measured at different depths, the cone tip resistance measured at CPT-3 and cone factor of $N_k = 10$ (see Figure 4.2) was used to estimate the VST undrained shear strength at the post-blast VST locations. The comparison of initial and post-blast results indicates that post-blast undrained shear strength associated with excess pore pressure ratios of 12.6 to 17.5% reduced by approximately 44 to 50%. Furthermore, Figure 4.8 shows that the peak undrained shear strength following the blast program is of the

same magnitude as the initial, residual undrained shear strength; thus, VST measurements of the peak and residual undrained shear strength of plastic, fine grained soils performed to support the design of planned transportation infrastructure can provide information suitable for evaluating the post-earthquake stability of structures founded within or above these deposits for excess pore pressures similar to those generated during the blasting program.

Based on these test results, it is concluded that the generation of excess pore pressures significantly below the typical magnitudes associated with full liquefaction can result in significant loss of strength within the plastic silts evaluated, with significant implications for the modeling of global stability of structures founded within and above this and similar silt deposits.

Table 4.2. Vane Shear Test results for Post-Blast Peak and Residual Shear Strength Corrected for Rod Friction where Applicable.

Vane Shear Test No.	Depth (m/[ft.])	Peak undrained shear strength, su,fv (kPa/[psf])	Residual undrained shear strength, sur,fv (kPa/[psf])	Representative plastic index, *PI*	Corrected peak undrained shear strength, su (kPa/[psf])	Corrected residual undrained shear strength, sur (kPa/[psf])	Sensitivity, ST
1	9.64 [31.61]	40.4 [844]	3.7 [78]	26	39.3 [821]	3.6 [76]	10.9
2	10.14 [33.28]	38.9 [812]	2.5 [52]	26	37.8 [791]	2.4 [51]	15.6
3[1]	10.64 [34.92]	–	–	30	–	–	–
4[1]	11.14 [36.56]	–	–	30	–	–	–
5[1]	11.64 [38.20]	–	–	30	–	–	–
6[2]	12.14 [39.84]	N/a	N/a	*NP*[3]	–	–	–

[1] Significant rod friction prevented reasonable interpretation of results.
[2] This test likely conducted in the sand layer typically encountered at this test.
[3] NP = non-plastic (clean sand)

Table 4.3. Comparison of initial and post-blast peak undrained shear strength within the silt layer.

Vane Shear Test No.	Depth (m/[ft])	Initial peak undrained shear strength (correlated to CPT with N_k = 10), s_u (kPa/[psf])	Post-blast, peak undrained shear strength measured with VST, s_u (kPa/[psf])	Reduction in undrained shear strength (%)
1	9.64 [31.61]	78.2 [1,630]	39.3 [821]	49.7
2	10.14 [33.28]	73.8 [1,540]	37.8 [791]	44.2

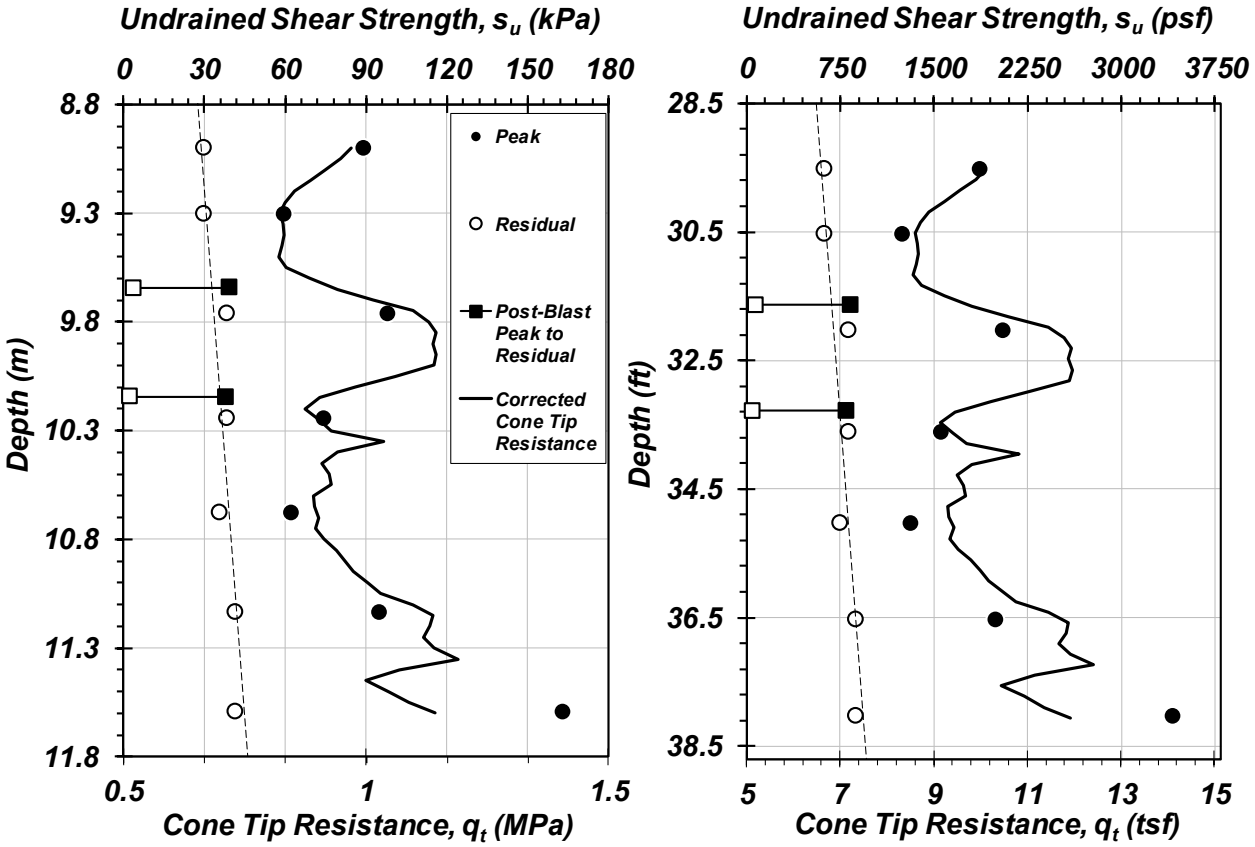

Figure 4.8. Comparison of peak and residual undrained shear strength measured following the 30 second blast sequence at borehole V-2 with depth to the pre-blast VST results measured at borehole V1: (left) metric units, and (right) imperial units.

5.0 CONCLUSIONS

This research report focused on the undrained shear strength of plastic silts soils subject to raised excess pore pressures, such as those anticipated following strong ground motion associated with the rupture of faults present within or separating tectonic plates. The knowledge of the possible reduction in undrained shear strength of soils is useful for planning and executing construction of transportation infrastructure subject to earthquake shaking. Testing of soils *in situ*, for example in the manner conducted in the research described in this study, presents certain advantages including the minimization of sample disturbance, the evaluation of large volumes of soil under realistic drainage conditions, and the observation of soil response under actual mechanical, hydrogeological, and thermal conditions of natural soil deposits.

The results of this study showed that for excess pore pressures equal to 12.6 to 17.5% of the *in situ* vertical effective overburden stress, the plastic silt deposit forming the subject of this investigation resulted in a loss of undrained shear strength ranging from 44 to 50%. The post-blasting undrained shear strength associated with the raised excess pore pressure field was determined equal to the initial, residual undrained shear strength as observed using the vane shear test. Although site-specific analyses are necessary to determine the magnitude of excess pore pressure possible for a given plastic soil under a given earthquake loading scenario, the results of this work indicate that substantial loss of soil strength may be anticipated following strong ground motion, and that commonly-available *in situ* strength measurements can provide a reasonable approximation of the strength conditions following an earthquake based on the results of this investigation.

6.0 REFERENCES

ASTM International (2019). *Standard Test Method for Field Vane Shear Test in Saturated Fine-Grained Soils*, (Standard No. D2573/D2573M – 18), West Conshohocken, PA: ASTM International,

Atwater, B. F., Musumi-Rokkaku, S., Satake, K., Tsuji, Y., Ueda, K., & Yamaguchi, D. K. (2005). *The Orphan Tsunami of 1700—Japanese clues to a parent earthquake in North America* (1707). Reston, VA: U.S. Geological Survey. https://doi.org/10.3133/pp1707

Boulanger, R. W., & Idriss, I. M. (2006). Liquefaction susceptibility criteria for silts and clays. *Journal of Geotechnical and Geoenvironmental Engineering*, *132*(11), 1413–1426. https://doi.org/10.1061/(asce)1090-0241(2006)132:11(1413)

Chandler, R. J. (1988). *The In-situ measurement of the undrained shear strength of clays using the field vane*, (Standard No. ASTM STP 1014). West Conshohocken, PA: ASTM International. https://doi.org/10.1520/STP10319S

General Electric Oil & Gas. (2009). *UNIK 5000 Pressure Sensing Platform Datasheet*.

Gianella, T. N. (2015). *Ground improvement and liquefaction mitigation using driven timber piles* (Doctoral dissertation, Oregon State University, 2015). Corvallis, OR: Oregon State University.

Gianella, T. N., & Stuedlein, A. W. (2017). Performance of driven displacement pile–Improved ground in controlled blasting field tests. *Journal of Geotechnical and Geoenvironmental Engineering*, *143*(9), 04017047. https://doi.org/10.1061/(asce)gt.1943-5606.0001731

Goldfinger, C., Nelson, C. H., Morey, A. E., Johnson, J. E., Patton, J. R., Karabanov, E., ... & Enkin, R. J. (2012). Turbidite event history: Methods and implications for Holocene paleoseismicity of the Cascadia subduction zone (Report No. 1661-F). Reston, VA: US Geological Survey. https://doi.org/10.3133/pp1661F

Holtz, R. D., Kovacs, W. D., & Sheahan, T. C. (2011). *An introduction to geotechnical engineering 2nd edition* (2nd ed.). Upper Saddle River, NJ: Pearson Education.

Kulhawy, F. H., & Mayne, P. W. (1990). *Manual on estimating soil properties for foundation design*. Palo Alto, CA: Electric Power Research Institute.

Mikkelsen, P., & Green, G. (2003). Piezometers in fully grouted boreholes. In *Proceedings of the Sixth International Symposium on Field Measurements in Geomechanics: 15-18 September, 2003, Oslo, Norway*. Boca Raton, FL: CRC Press.

Rollins, K. M., Lane, J. D., Dibb, E., Ashford, S. A., & Mullins, A. G. (2005). Pore pressure measurement in blast-induced liquefaction experiments. *Transportation Research Record: Journal of the Transportation Research Board*, *1936*(1), 210–220. https://doi.org/10.1177/0361198105193600124

Rollins, K. M., & Anderson, J. K. (2008). Cone penetration resistance variation with time after blast liquefaction testing. *Geotechnical Earthquake Engineering and Soil Dynamics IV,* (181), 1-10. doi:10.1061/40975(318)103

Suits, L. D., Sheahan, T. C., Cox, B. R., Stokoe, K. H., & Rathje, E. M. (2009). An in Situ test method for evaluating the coupled pore pressure generation and nonlinear shear modulus behavior of liquefiable soils. *Geotechnical Testing Journal*, *32*(1), 101484. https://doi.org/10.1520/gtj101484

Van Ballegooy, S., Roberts, J., Stokoe, K., Cox, B., Wentz, F., & Hwang, S. (2015). Large-scale testing of shallow ground improvements using controlled staged-loading with T-Rex. In *6th International Conference on Earthquake Geotechnical Engineering 1-4 November 2015 Christchurch, New Zealand*. London, United Kingdom: International Society for Soil Mechanics and Geotechnical Engineering.